https://doi.org/10.5194/wes-2026-171
Preprint. Discussion started: 3 November 2026
© Author(s) 2026. CC BY 4.0 License.



eawe european academy of wind energy
Open Access WIND ENERGY SCIENCE DISCUSSIONS

Spectral Prediction of Pitch Rate Distribution for Actuator Duty Cycle and Rate Saturation Probability Estimation under Individual Pitch Control

Daniel Lacheta-Lecumberri[1,2], Irene Miquelez-Madariaga[2], and Jorge Elso[2]

[1]Vors Control Technology S.L., Pamplona, Spain
[2]Department of Engineering, Universidad Pública de Navarra, Pamplona, Spain

Correspondence: Daniel Lacheta-Lecumberri (dlacheta@vorscontrol.com)

Abstract. Pitch actuator usage under Individual Pitch Control is typically assessed *a posteriori* through computationally expensive aeroelastic simulations. This work proposes a spectral methodology to predict the pitch rate probability density function during linear control design stage, enabling the estimation of actuator duty cycle and rate saturation probability. The pitch rate is characterized as a Sine-on-Random process whose deterministic and stochastic parameters are estimated from operating point values, equivalent disturbance spectra and closed-loop transfer functions. Validation on the IEA 15 MW Reference Wind Turbine under turbulent inflow shows maximum errors of 0.79% and 0.59% for both indicators, respectively, providing an efficient methodology for designing linear controllers that explicitly account for actuator usage and limitations, while reducing reliance on iterative aeroelastic simulations.

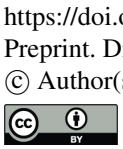
1 Introduction

The continuous upscaling of wind turbines has contributed substantially to the growth of wind energy installed capacity by increasing energy capture and reducing generation costs (Henrique et al., 2025). However, larger rotor are exposed to greater spatial variability of the inflow, increasing asymmetric structural loads and the need for effective control strategies to reduce them (Canet et al., 2021; Bošnjaković et al., 2022). At the same time, longer and heavier blades impose increasingly demanding requirements on pitch actuators, mainly because of their rotational inertia and pitching loads (Jeong et al., 2025). These requirements can significantly affect the sizing and cost of the pitch system (Pusch et al., 2024). Consequently, modern wind turbines face a growing need for asymmetric load reduction while capabilities of their pitch actuators are increasingly constrained.

In this context, Individual Pitch control (IPC) is one of the most established strategies for mitigating asymmetric loads (Bossanyi, 2003). However, its load reduction effect is followed by a substancial increase in pitch actuator activity (Bossanyi, 2005). Therefore, a direct trade-off exists between structural load mitigation and actuator usage, making pitch actuator limitations particularly relevant when designing IPC strategies.

In conventional control design, this trade-off is generally assessed *a posteriori* through aeroelastic simulations. After the controller is designed, its load reduction performance and actuator usage are evaluated. If the resulting compromise is not

https://doi.org/10.5194/wes-2026-171
Preprint. Discussion started: 3 November 2026
© Author(s) 2026. CC BY 4.0 License.



eawe european academy of wind energy
Open Access WIND ENERGY SCIENCE DISCUSSIONS

acceptable, the controller is retuned and the simulations are repeated. As illustrated in Figure 1, this leads to an iterative design and validation process in which computationally expensive aeroelastic simulations remain within the controller tuning loop.

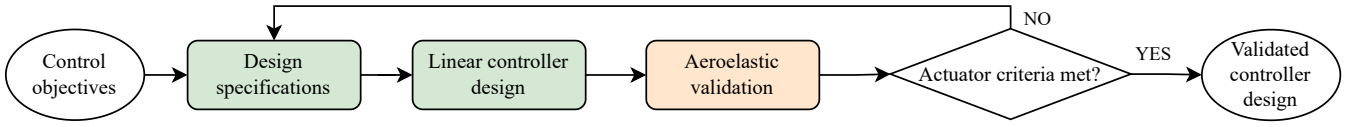


Figure 1. Definition of the blade rotating frame (blue) and the rotor fixed frame (red).

The increasing relevance of pitch actuator constraints has motivated the development of control strategies that account for actuator behavior during controller design. Existing approaches can be broadly classified into two groups. The first one comprises IPC formulations aimed at reducing actuator activity, commonly quantified through the actuator duty cycle (ADC) indicator, while maintaining the load reduction performance. The second group focuses on the explicit treatment of physical actuator constraints, particularly rate limitations, either by mitigating the effects of saturation or by incorporating the constraints directly into the control formulation.

Within the first approach, Vali et al. (2016) developed a MIMO IPC architecture which improves both load redution and actuator utilization compared with a conventional SISO formulation. Similarly, Aktan and Bottasso (2023) introduced a non-linear PI controller that reduces the actuator duty cycle (ADC) while maintaining the load reduction performance against a conventional PI controller. More recently, several output-constrained IPC schemes have been proposed to optimize the trade-off between actuator usage and load mitigation. These include the constrained subspace predictive repetitive control (cSPRC) proposed by Liu et al. (2022) and the ℓ^∞ and ℓ^2-based formulations developed in Hummel et al. (2025). Other studies have also achieved reductions in actuator activity through the use of virtual actuators (Hovgaard et al., 2024) or by introducing an azimuth offset in the inverse Multi-Blade Coordinate (MBC) transformation to improve the decoupling between the IPC control actions (Mulders et al., 2019).

The second approach addresses the physical constraints of the pitch actuator more explicitly. Within this category, anti-windup schemes are used to mitigate performance degradation and potential instability once actuator saturation occurs (Kanev, 2009; Unguran et al., 2019; Wang and Gambier, 2021). Although these methods improve the closed-loop response under saturation, actuator constraints are not generally considered during the design of the controller. Other approaches incorporate these limitations more explicitly into the control design. Model predictive control (MPC) can directly impose actuator constraints within the optimization problem (Petrović et al., 2021; Liu et al., 2021), whereas preview control strategies use information about incoming disturbances to anticipate the required pitch action and facilitate compliance with actuator limits (Laks et al., 2010).

Despite these developments, no general and computationally efficient framework is avaliable for predicting actuator usage during the design of conventional linear controllers. Actuator related quantities are still commonly evaluated *a posteriori* from aeroelastic simulations, while their explicit consideration during controller design may require complex control architectures

https://doi.org/10.5194/wes-2026-171
Preprint. Discussion started: 3 November 2026
© Author(s) 2026. CC BY 4.0 License.



eawe european academy of wind energy
Open Access WIND ENERGY SCIENCE DISCUSSIONS

or additional sensing systems. Therefore, a predictive framework is needed to support controller tuning and enable candidate control configurations to be compared before aeroelastic validation.

Previous studies have shown that statistical properties of wind turbine signals can be predicted during linear controller design by combining disturbance spectra with closed-loop transfer functions, for example to formulate fatigue-related design specifications (Hammerum et al., 2007; Miquelez-Madariaga et al., 2026). Following this approach, the authors previously proposed a spectral methodology to estimate pitch actuator rate saturation probability during linear controller design (Lacheta-Lecumberri et al., 2026b). Under a Gaussian assumption of the pitch rate probability density function (PDF), the method combines the disturbance spectrum and the closed-loop transfer function to estimate the probability of exceeding the actuator rate limit. This work provides the basis for the design workflow shown in Figure 2, in which statistical indicators of actuator usage are introduced as design criteria to support controller tuning and the comparison of control configurations reducing reliance on iterative aeroelastic simulations.

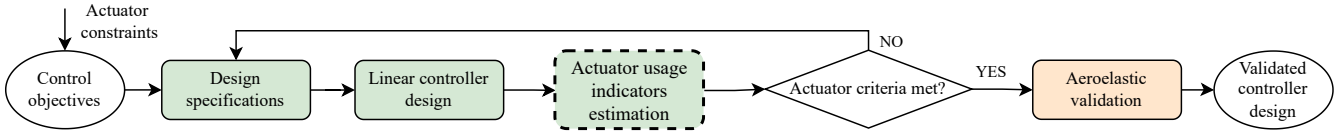


Figure 2. Definition of the blade rotating frame (blue) and the rotor fixed frame (red).

However, the previous formulation was developed for collective pitch actions, for which the assumption of Gaussianity in the pitch rate signal was appropiate. Extending this approach to IPC is not straightforward. IPC control actions are generated in the fixed frame while actuator constraints are defined in the rotating frame. Moreover, the inverse MBC transformation introduces deterministic components to the pitch signal that may substantially modify the pitch rate distribution.

To address these challenges, this work extends the previous work by developing the prediction of the complete PDF of the individual blade pitch rate under IPC configurations. The pitch rate is analytically decomposed into a deterministic and a Gaussian stochastic contribution, allowing its distribution to be characterized through a Sine-on-Random (SoR) model. The deterministic and stochastic parameters are estimated from operating point values, equivalent disturbance spectra and closed-loop transfer functions. Once the pitch rate PDF is reconstructed, statistical indicators of actuator usage can be evaluated direclty during linear controller design, reducing reliance on iterative aeroelastic simulations. The methodology is then applied to predict pitch actuator duty cylce (ADC) and rate saturation probability (P_{sat}), and is validated against turbulent aeroelastic simulations for two IPC configurations.

The remainder of the paper is organized as follows. Section 2 provides an overview of the conventional IPC formulation, the equivalent disturbance framework and the SoR distribution. Section 3 presents the analytical characterization of the pitch rate distribution and the estimation of the statistical indicatiors from the predicted PDF. Section 4 validates the proposed methodology through turbulent aeroelastic simulations and Section 5 summarizes the main conclusions and describe future research directions.

https://doi.org/10.5194/wes-2026-171
Preprint. Discussion started: 3 November 2026
© Author(s) 2026. CC BY 4.0 License.



eawe european academy of wind energy
Open Access WIND ENERGY SCIENCE DISCUSSIONS

2 Theoretical background

This section summarizes the theoretical background required to predict the pitch rate distribution under Individual Pitch Control (IPC). The conventional IPC formulation is first introduced, establishing the fixed-frame representation of asymmetric pitch actions. Secondly, a equivalent disturbance framework is presented, enabling the spectral reconstruction of closed-loop signals through a three-disturbance MIMO representation. Finally, the Sine-on-Random (SoR) distribution is reviewed, providing the probabilistic framework used to describe signals containing both deterministic periodic and stochastic contributions.

2.1 Conventional IPC design

Conventional IPC implementations are formulated in the fixed-frame *0dq* reference system through the Multi-Blade Coordinate (MBC) transformation (Park, 1929). Given a set of blade signals expressed in the rotating frame $M_{123}(t) = [M_1(t), M_2(t), M_3(t)]^T$, the direct MBC transformation $T(\psi(t))$ is defined as

$$\begin{bmatrix} M_0(t) \\ M_d(t) \\ M_q(t) \end{bmatrix} = \underbrace{\frac{2}{3}\begin{bmatrix} 1/2 & 1/2 & 1/2 \\ \cos(\psi(t)) & \cos\left(\psi(t)+\frac{2\pi}{3}\right) & \cos\left(\psi(t)+\frac{4\pi}{3}\right) \\ \sin(\psi(t)) & \sin\left(\psi(t)+\frac{2\pi}{3}\right) & \sin\left(\psi(t)+\frac{4\pi}{3}\right) \end{bmatrix}}_{T(\psi(t))} \begin{bmatrix} M_1(t) \\ M_2(t) \\ M_3(t) \end{bmatrix}, \tag{1}$$

where $\psi(t)$ denotes the rotor azimuth angle of the reference blade. Figure 3 illustrates the relationship between the rotating blade frame and the fixed frame. Asymmetric blade moments are projected onto two virtual load components, M_d and M_q, associated with the tilt and yaw directions of the rotor, respectively. This transformation converts once-per-revolution load variations into slowly varying signals, enabling the application of standard linear control techniques.

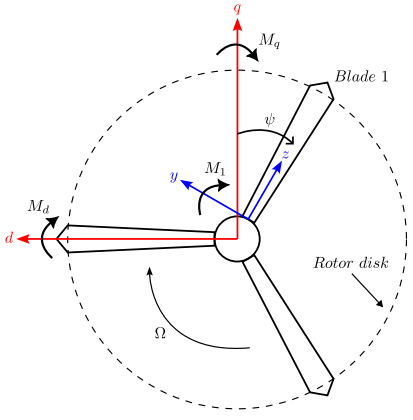


Figure 3. Definition of the blade rotating frame (blue) and the rotor fixed frame (red).

IPC controllers act on M_d and M_q to generate virtual pitch commands β_d and β_q, whereas M_0 is generally excluded from the IPC strategy. For the design of these controllers, the linearized wind turbine model is also transformed into *0dq* frame (Bir, 2008), yielding the block diagram depicted in Figure 4.

https://doi.org/10.5194/wes-2026-171
Preprint. Discussion started: 3 November 2026
© Author(s) 2026. CC BY 4.0 License.



eawe european academy of wind energy
Open Access WIND ENERGY SCIENCE DISCUSSIONS

The virtual pitch commands are subsequently transformed back to individual blade pitch references through the inverse MBC transformation $T^{-1}(\psi(t))$,

$$\begin{bmatrix}\beta_1(t)\\ \beta_2(t)\\ \beta_3(t)\end{bmatrix} = \underbrace{\begin{bmatrix}1 & \cos(\psi(t)) & \sin(\psi(t))\\ 1 & \cos\left(\psi(t)+\frac{2\pi}{3}\right) & \sin\left(\psi(t)+\frac{2\pi}{3}\right)\\ 1 & \cos\left(\psi(t)+\frac{4\pi}{3}\right) & \sin\left(\psi(t)+\frac{4\pi}{3}\right)\end{bmatrix}}_{T^{-1}(\psi(t))} \begin{bmatrix}\beta_0(t)\\ \beta_d(t)\\ \beta_q(t)\end{bmatrix}, \tag{2}$$

where $\beta_0(t)$ denotes the collective pitch command typically generated by the rotor speed controller. The resulting individual blade pitch references are then applied to each pitch actuator system, producing blade pitch actions aimed at mitigating asymmetric structural loads.

2.2 Equivalent disturbance framework

To enable the spectral analysis and estimation of asymmetric signals of the system, the equivalent disturbance framework proposed in Lacheta-Lecumberri et al. (2026a) is adopted. The distributed aerodynamic excitation is represented by three equivalent disturbances, denoted by W_0^{eq}, W_d^{eq} and W_q^{eq}, associated with the collective, tilt and yaw components of the inflow, respectively. The resulting closed-loop representation shown in Figure 4, explicitly incorporates these disturbances as inputs to the wind turbine model, yielding a MIMO formulation suitable for spectral analyses.

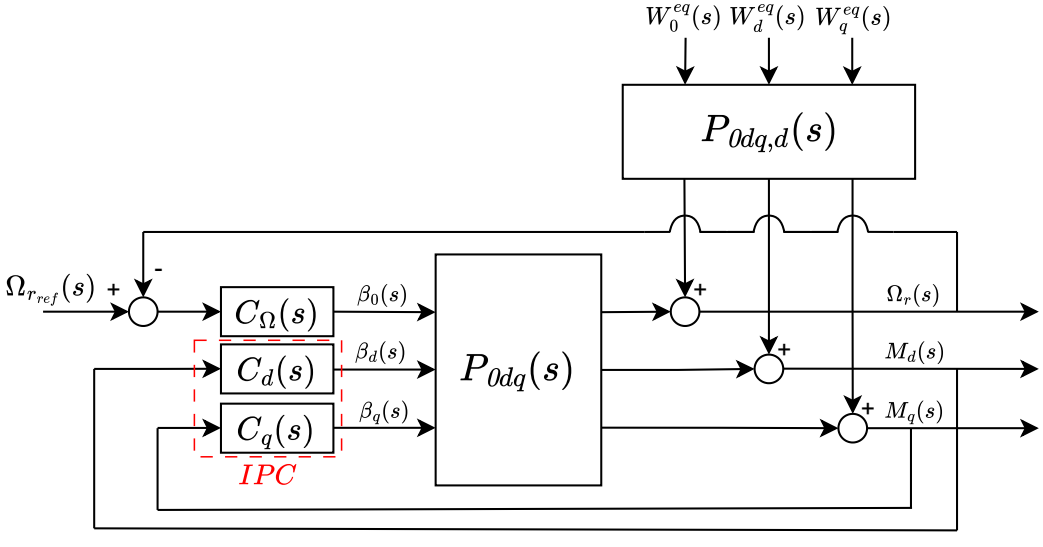


Figure 4. Augmented diagram block including the equivalent wind disturbances, used for the spectral propagation and output estimation, and proposed for advanced control designs.

https://doi.org/10.5194/wes-2026-171
Preprint. Discussion started: 3 November 2026
© Author(s) 2026. CC BY 4.0 License.



eawe european academy of wind energy
Open Access WIND ENERGY SCIENCE DISCUSSIONS

Let $\mathbf{G}(j\omega)$ denote the closed-loop transfer matrix from the equivalent disturbances to the selected outputs. The output spectral matrix is estimated as

$$\mathbf{S}_{yy}(\omega) = \mathbf{G}(j\omega)\mathbf{S}_{ww}(\omega)\mathbf{G}^{H}(j\omega) \tag{3}$$

where $\mathbf{S}_{ww}(\omega) \in \mathbb{R}^{3\times3}$ is the spectral matrix of the equivalent disturbances and $(\cdot)^H$ denotes the Hermitian transpose (Ljung, 1987). It is assumed that the statistical properties of the equivalent disturbances remain invariant with respect to the control configuration under consideration and that the collective and asymmetric components are statistically independent, leading to

$$\mathbf{S}_{ww}(\omega) = \begin{bmatrix} S_{00}(\omega) & 0 & 0 \\ 0 & S_{dd}(\omega) & S_{dq}(\omega) \\ 0 & S_{qd}(\omega) & S_{qq}(\omega) \end{bmatrix}, \tag{4}$$

where $S_{00}(\omega)$, $S_{dd}(\omega)$ and $S_{qq}(\omega)$ are the auto-spectra of W_0^{eq}, W_d^{eq} and W_q^{eq}, respectively, while $S_{dq}(\omega)$ and $S_{qd}(\omega)$ denote the cross-spectra between the asymmetric components.

A key feature of this framework is that, once the equivalent disturbance spectra have been characterized from a baseline set of aeroelastic simulations, the PSDs of system signals can be estimated for alternative control configurations using only the corresponding closed-loop transfer functions. Consequently, the spectral response of both collective and asymmetric signals can be predicted without requiring additional aeroelastic simulations, providing direct access to their PSDs and associated statistical properties. In the present work, this capability is exploited to estimate the PSDs of the IPC pitch commands in the *0dq* frame, providing the basis for the pitch rate distribution estimation developed in the following sections.

2.3 Sine-on-Random (SoR) distribution

Let $x(t)$ be a process consisting of a sinusoidal component $y(t)$ of amplitude A and angular frequency ω_A, combined with a stationary Gaussian process $n(t)$. Figure 5a illustrates a representative realization of this type of signal. Assuming both components are statistically independent, the process can be expressed as

$$x(t) = y(t) + n(t) = A\cos(\omega_A t) + \sum_{p=1}^{P} \left[b_p \cos(\omega_p t) + c_p \sin(\omega_p t)\right]. \tag{5}$$

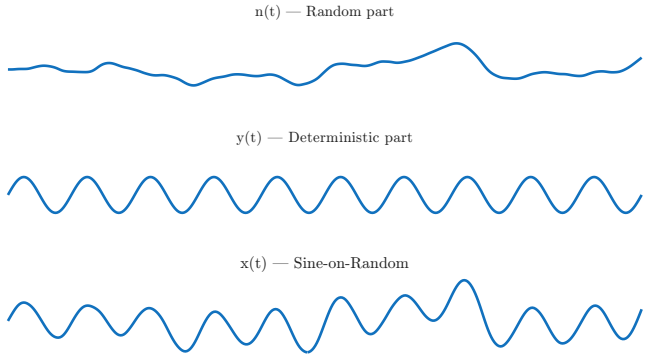
where $\omega_p = p\ d\omega$, being $d\omega$ the width of the frequency band associated with the p-th component, and b_p and c_p follow a Gaussian distribution with zero mean and standard deviation σ_n (Zucca et al., 2021), given by

$$\sigma_n^2 = \mathbb{E}\left[(n(t))^2\right]. \tag{6}$$

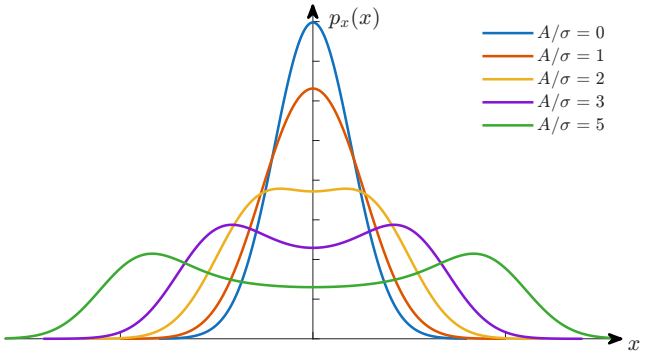
For a stationary process, the same quantity can be equivalently obtained from the signal power spectral density (PSD) as

$$\sigma_n^2 = \frac{1}{2\pi}\int_0^\infty S_{nn}(\omega)d\omega. \tag{7}$$

https://doi.org/10.5194/wes-2026-171
Preprint. Discussion started: 3 November 2026
© Author(s) 2026. CC BY 4.0 License.



(a) Temporal example of a SoR signal with $A/\sigma = 2$.



(b) Probability density function as a function of A/σ (adapted from Zucca et al. (2021)).

Figure 5. Temporal and probability distribution examples of SoR signals.

Although the probability density function (PDF), p_x, of x can be obtained either by convolving the individual distributions of the sinusoidal and Gaussian components or by computing the inverse Fourier transform of the corresponding characteristic function, the latter approach is adopted here due to its simpler formulation (Stephen O. Rice, 1945).

The characteristic funtion of x is given by

$$\phi_x(\zeta, A, \sigma) = \phi_y(\zeta, A)\phi_n(\zeta, \sigma) = J_0(A\zeta)\exp\left(-\frac{\sigma^2\zeta^2}{2}\right). \tag{8}$$

where J_0 denotes the Bessel function of order zero.

Applying the inverse Fourier transform yields the probability density function

$$p_x(x, A, \sigma) = \frac{1}{\pi}\int_0^\infty \phi_x(\zeta, A, \sigma)\cos(x\zeta)d\zeta. \tag{9}$$

As can be observed, the distribution depends only on the sinusoidal amplitude A and the standard deviation of the Gaussian component σ. Figure 5b compares several values of the ratio A/σ. When the Gaussian component dominates ($A/\sigma \ll 1$), the distribution converges towards a normal distribution. But, as the sinusoidal component becomes dominant, the distribution progressively differs from Gaussianity and presents heavier tails.

Once the PDF is defined, probability-based quantities can be computed by integrating the distribution over the corresponding range of values (Feller, 1957). For instance, expected values of functions of the signal can be obtained directly from the PDF. For a generic function $g(x)$, the expected value is defined as

$$\mathbb{E}[g(x)] = \int_{-\infty}^{\infty} g(x)\, p_x(x, A, \sigma)\, dx. \tag{10}$$

https://doi.org/10.5194/wes-2026-171
Preprint. Discussion started: 3 November 2026
© Author(s) 2026. CC BY 4.0 License.



eawe european academy of wind energy
Open Access WIND ENERGY SCIENCE DISCUSSIONS

Similarly, the probability of exceeding the value q can be computed by integrating the PDF between this value and infinite as

$$P(X > q) = \int_{q}^{\infty} p_x(x, A, \sigma)\, dx. \tag{11}$$

These properties enable the direct computation of actuator-related indicators from the predicted pitch rate PDF. In the following sections, they are used to estimate the Actuator Duty Cycle (ADC) and the rate saturation probability for different control configurations without relying on time-domain aeroelastic simulations.

3 Pitch rate distribution under IPC

The periodic pitch activity introduced by IPC modifies the statistical distribution of the pitch rate signal with respect to conventional collective control scenarios. As a result, the Gaussian approximation may no longer be sufficient and a more general distribution model is required to describe the pitch rate behavior under IPC.

To this end, Section 3.1 derives an analytical decomposition of the IPC pitch rate signal into deterministic and stochastic components. Based on this decomposition, Section 3.2 presents the estimation of the SoR parameters directly from the operating point steady-state values, the closed-loop transfer functions and the equivalent disturbance spectra introduced in Section 2.2. Finally, in Section 3.3, actuator usage indicators are computed from the estimated pitch rate PDF.

3.1 Analytical decomposition of pitch rate

Since pitch actuator limitations affect to the individual blade pitch signals, the analysis must be conducted in the rotating frame. Therefore, the starting point is the application of (2), which relates the individual blade pitch commands to the collective and IPC control actions generated in fixed-frame coordinates.

Assuming constant rotor speed and zero initial azimuth angle, such that $\psi(t) = \Omega t$, the pitch command for blade 1 is given by

$$\beta_1(t) = \beta_0(t) + \beta_d(t)\cos(\Omega t) + \beta_q(t)\sin(\Omega t)\,. \tag{12}$$

Differentiating this expression with respect to time yields

$$\dot{\beta}_1(t) = \dot{\beta}_0(t) + \dot{\beta}_d(t)\cos(\Omega t) + \dot{\beta}_q(t)\sin(\Omega t) + \Omega\left[\beta_q(t)\cos(\Omega t) - \beta_d(t)\sin(\Omega t)\right]. \tag{13}$$

In order to understand the statistical nature of this expression, each fixed frame command is decomposed into a constant $\bar{(\cdot)}$ and a fluctuating component $\tilde{(\cdot)}$.

Starting with the contribution associated with the mean values, only the constant terms of the pitch commands are retained in the pitch rate expression, yielding the following deterministic contribution to the blade pitch rate signal

$$\dot{\beta}_{1,\mathrm{det}}(t) = \Omega\left[\bar{\beta}_q\cos(\Omega t) - \bar{\beta}_d\sin(\Omega t)\right], \tag{14}$$

https://doi.org/10.5194/wes-2026-171
Preprint. Discussion started: 3 November 2026
© Author(s) 2026. CC BY 4.0 License.



eawe european academy of wind energy
Open Access WIND ENERGY SCIENCE DISCUSSIONS

which can be rewritten as a single sinusoidal component as

$$\dot{\beta}_{1,\mathrm{det}}(t) = A\sin(\Omega t + \phi), \tag{15}$$

where

$$A = \Omega\sqrt{\bar{\beta}_d^2 + \bar{\beta}_q^2}, \tag{16}$$

and ϕ is a constant phase shift. Thus, the mean values of the IPC pitch commands generate a deterministic harmonic component in the blade pitch rate signal at the rotor frequency Ω. The amplitude of this contribution is fully determined by the constant components of the *dq* pitch commands through the parameter *A*.

The stochastic contribution $\dot{\beta}_{1,\mathrm{fluc}}(t)$ is given by the fluctuating components of (13) which depend on the closed-loop response of the collective and IPC control loops. This leads to

$$\dot{\beta}_{1,\mathrm{fluc}}(t) = \dot{\tilde{\beta}}_0(t) + \dot{\tilde{\beta}}_d(t)\cos(\Omega t) + \dot{\tilde{\beta}}_q(t)\sin(\Omega t) + \Omega\left[\tilde{\beta}_q(t)\cos(\Omega t) - \tilde{\beta}_d(t)\sin(\Omega t)\right]. \tag{17}$$

The complete pitch rate signal can therefore be expressed as the superposition of a deterministic sinusoidal and a stochastic component,

$$\dot{\beta}_1(t) = \dot{\beta}_{1,\mathrm{det}}(t) + \dot{\beta}_{1,\mathrm{fluc}}(t). \tag{18}$$

Assuming that the stochastic contribution can be approximated as a Gaussian process, the resulting pitch rate signal is consistent with the Sine-on-Random formulation introduced in Section 2.3. Therefore, the statistical characterization of the signal reduces to the estimation of the deterministic amplitude *A* and the standard deviation σ of the stochastic contribution.

3.2 Estimation of SoR parameters

Once the pitch rate signal under IPC is decomposed into the sum of a deterministic periodic component and a stochastic component, its statistical distribution can be represented using the SoR formulation introduced in Section 2.3 as

$$p_{\dot{\beta}_1}(\dot{\beta}_1, A, \sigma) = \frac{1}{\pi}\int_0^\infty \phi_{\dot{\beta}_1}(\zeta, A, \sigma)\cos(\dot{\beta}_1\zeta)d\zeta. \tag{19}$$

Therefore, the estimation of this distribution reduces to detemining the two parameters defining the PDF: the amplitude of the deterministic component *A*, and the standard deviation of the stochastic component, σ. The following subsections present analytical procedures for estimating both quantities directly from the closed-loop spectral representation of the system.

3.2.1 Deterministic component A

As shown in the previous subsection, the deterministic component of the IPC pitch rate signal is determined by the mean values of the virtual commands in the fixed frame. These values are originated from the periodic pitch activity inherently required to compensate for the asymmetric loading present at the operating point (op). Provided that the closed-loop system is stable, the

https://doi.org/10.5194/wes-2026-171
Preprint. Discussion started: 3 November 2026
© Author(s) 2026. CC BY 4.0 License.



eawe european academy of wind energy
Open Access WIND ENERGY SCIENCE DISCUSSIONS

mean values of the virtual pitch commands $\bar{\beta}_{d,q}$ are determined by the operating point conditions and are independent of the particular IPC controller design.

Let $\mathbf{G}(0)$ denote the steady-state gain matrix of the linearized wind turbine model, relating the virtual pitch β_{dq} commands to the fixed frame load components M_{dq} and let $M_{d,ref}$ and $M_{q,ref}$ denote the IPC load references (typically set to zero). Under this asumption, the operating point values of the IPC pitch commands are obtained from

$$\begin{bmatrix} \beta_{d,op} \\ \beta_{q,op} \end{bmatrix} = \mathbf{G}(0)^{-1} \begin{bmatrix} M_{d,ref} - M_{d,op} \\ M_{q,ref} - M_{q,op} \end{bmatrix}, \tag{20}$$

which yields

$$\beta_{d,op} = \frac{(M_{d,ref} - M_{d,op})G_{qq}(0) - (M_{q,ref} - M_{q,op})G_{dq}(0)}{G_{dd}(0)G_{qq}(0) - G_{dq}(0)G_{qd}(0)}, \tag{21}$$

and

$$\beta_{q,op} = \frac{(M_{q,ref} - M_{q,op})G_{dd}(0) - (M_{d,ref} - M_{d,op})G_{qd}(0)}{G_{dd}(0)G_{qq}(0) - G_{dq}(0)G_{qd}(0)}. \tag{22}$$

Since the operating point values correspond to the mean values of the virtual pitch commands, the deterministic amplitude A defined in (16) can be directly written as

$$A = \Omega_{1P}\sqrt{\beta_{d,op}^2 + \beta_{q,op}^2} \tag{23}$$

where Ω_{1P} denotes the rotor rotational speed, which can be defined through the operating point values too. Therefore, the parameter A can be determined directly from the operating point loads and the steady-state gains of the linearized plant, without requering knowledge of the specific IPC controller tuning.

3.2.2 Stochastic component σ

According to the decomposition derived in Section 3.1, the stochastic contribution of the blade pitch rate signal is given by (17). Within the SoR framework, σ is defined as the standard deviation of this fluctuating contribution. Therefore, the objective of this subsection is to derive an analytical expression for the variance of $\dot{\tilde{\beta}}_1(t)$ in terms of the statistical properties of the collective and IPC pitch signals.

For notational simplicity, the tilde notation is omitted in the remainder of the subsection. Therefore, all variables in the following derivation refer to their zero-mean fluctuating components.

The derivation assumes stationary zero-mean pitch fluctuations, an statistically constant rotor speed and a rotor azimuth uniformly distributed over $[0, 2\pi]$ for sufficiently long observation intervals.

Following (6), the variance of the stochastic component is computed from (17) as

$$\sigma_{\dot{\beta}_1}^2 = \mathbb{E}\left[\dot{\beta}_1^2(t)\right]. \tag{24}$$

https://doi.org/10.5194/wes-2026-171
Preprint. Discussion started: 3 November 2026
© Author(s) 2026. CC BY 4.0 License.



eawe european academy of wind energy
Open Access WIND ENERGY SCIENCE DISCUSSIONS

After expanding the expression, variance and covariance properties are applied. Under the assumption of uniformly distributed azimuth, the trigonometric terms introduced by the inverse MBC transformation satisfy

$$\mathbb{E}\left[\sin(\Omega t)\right] = \mathbb{E}\left[\cos(\Omega t)\right] = \mathbb{E}\left[\sin(\Omega t)\cos(\Omega t)\right] = 0, \qquad \mathbb{E}\left[\cos^2(\Omega t)\right] = \mathbb{E}\left[\sin^2(\Omega t)\right] = 1/2. \tag{25}$$

Through these relations, the variance of the stochastic pitch rate contribution is obtained as

$$\sigma^2_{\dot{\beta}_1} = \sigma^2_{\dot{\beta}_0} + \frac{1}{2}\left(\sigma^2_{\dot{\beta}_d} + \sigma^2_{\dot{\beta}_q}\right) + \frac{1}{2}\Omega^2\left(\sigma^2_{\beta_d} + \sigma^2_{\beta_q}\right) + 2\Omega\,\mathrm{Cov}(\dot{\beta}_d, \beta_q). \tag{26}$$

This expression provides a direct analytical way to compute the standard deviation of the stochastic blade pitch rate component in the rotating frame from the variances of the pitch commands expressed in the fixed frame and the covariance term coupling the *dq* axes. Its practical relevance lies in the fact that all the variance and covariance terms of the expression can be obtained from the PSD of the corresponding fixed-frame signals.

Based on (7), the variance of the time derivative of a pitch command can be obtained by multiplying its PSD by ω^2 as

$$\sigma^2_{\dot{\beta}_i} = \frac{1}{2\pi}\int_0^\infty \omega^2 S_{\beta_i\beta_i}(\omega)\,d\omega, \qquad i \in \{0, d, q\}. \tag{27}$$

Similarly, the covariance term can be obtained from the corresponding cross-spectral density as

$$\mathrm{Cov}(\dot{\beta}_d, \beta_q) = -\frac{1}{2\pi}\int_0^\infty \omega\,\mathrm{Im}\left(S_{\beta_d\beta_q}(\omega)\right)d\omega. \tag{28}$$

Since all the terms in (26) can be obtained from auto-spectral and cross-spectral densities (CPSDs), the stochastic parameter of the SoR distribution can be estimated entirely in the frequency domain. In particular, the required PSDs and CPSDs of the fixed-frame pitch commands can be predicted using the equivalent-disturbance framework introduced in Section 2.2. By propagating the PSDs of the equivalent disturbances through the corresponding closed-loop transfer matrix, the variances required can be obtained without performing additional aeroelastic simulations for each control configuration.

Although the derivation is presented for blade 1, the remaining blades differ only through the constant phase shifts introduced by the inverse MBC transformation. Since the expected values of the trigonometric functions are invariant to a constant phase shift, it can be assumed that the three blades have the same stochastic pitch rate variance under the adopted assumptions. The same reasoning applies when a constant azimuth offset is included in the inverse MBC transformation (Mulders et al., 2019).

3.3 Actuator indicators from the predicted pitch rate PDF

Once the pitch rate PDF has been reconstructed from the estimated SoR parameters, several statistical conclusions can be drawn regarding actuator usage for a given control configuration. In particular, actuator-related indicators can be computed by integrating the distribution over the corresponding ranges of interest. This enables quantities normally evaluated from time-domain simulations to be predicted during the linear control design stage. The following subsections define the two indicators considered in this work: the pitch actuator duty cycle (ADC) and the pitch actuator rate saturation probability.

https://doi.org/10.5194/wes-2026-171
Preprint. Discussion started: 3 November 2026
© Author(s) 2026. CC BY 4.0 License.



eawe european academy of wind energy
Open Access WIND ENERGY SCIENCE DISCUSSIONS

3.3.1 Estimation of pitch actuator duty cycle

The pitch actuator duty cycle (ADC) is commonly used to quantify the average use of the pitch actuator rate over a given time interval (Bottasso et al., 2013). This definition provides a normalized measure of the average actuator rate demand with respect to the available rate capability. For a pitch rate signal $\dot{\beta}(t)$ and a maximum actuator rate R_{max}, it is typically computed from time-domain data as

$$ADC(\beta_1) = \frac{1}{T}\int_0^T \frac{|\dot{\beta}_1(t)|}{R_{max}} dt. \tag{29}$$

Equivalently, the ADC can be interpreted as the time average of the absolute pitch rate signal, normalized by the actuator rate limit. For sufficiently long signals, this time average can be approximated by the expected value of the absolute pitch rate as

$$\frac{1}{T}\int_0^T |\dot{\beta}_1(t)| \approx \mathbb{E}[|\dot{\beta}_1|]. \tag{30}$$

Once the pitch rate PDF has been estimated, this expected value can be computed directly from the distribution following (10) with $g(x) = |\dot{\beta}_1|$ as

$$\mathbb{E}[|\dot{\beta}_1|] = \int_{-\infty}^{\infty} |\dot{\beta}_1| \cdot p_{\dot{\beta}_1}(\dot{\beta}_1, A, \sigma) d\dot{\beta}_1. \tag{31}$$

Therefore, the actuator duty cycle can be predicted from the estimated pitch rate PDF as

$$\widehat{ADC}(\beta_1) = \frac{\mathbb{E}[|\dot{\beta}_1|]}{R_{max}} = \frac{1}{R_{max}} \int_{-\infty}^{\infty} |\dot{\beta}_1| \cdot p_{\dot{\beta}_1}(\dot{\beta}_1, A, \sigma) d\dot{\beta}_1. \tag{32}$$

This formulation allows the ADC to be evaluated without requiring pitch rate time signals. Instead, the indicator is obtained from the predicted pitch rate distribution, enabling ADC to be assessed during the linear controller design stage.

3.3.2 Estimation of pitch actuator rate saturation probability

The pitch actuator rate saturation probability quantifies the likelihood that the blade pitch rate demand exceeds the actuator rate capability. This probability can be obtained by integrating the tails of the pitch rate PDF outside the admissible rate range. When the positive and negative actuator rate limits are asymmetric, denoted by R^+_{max} and R^-_{max}, respectively, the estimated rate saturation probability can be computed by integrating the two tails of the pitch rate PDF as

$$\hat{P}_{sat} = P(\dot{\beta}_1 < R^-_{max}) + P(\dot{\beta}_1 > R^+_{max}) = \int_{-\infty}^{R^-_{max}} p_{\dot{\beta}_1}(\dot{\beta}_1, A, \sigma) d\dot{\beta}_1 + \int_{R^+_{max}}^{\infty} p_{\dot{\beta}_1}(\dot{\beta}_1, A, \sigma) d\dot{\beta}_1. \tag{33}$$

https://doi.org/10.5194/wes-2026-171
Preprint. Discussion started: 3 November 2026
© Author(s) 2026. CC BY 4.0 License.



eawe european academy of wind energy
Open Access WIND ENERGY SCIENCE DISCUSSIONS

For the common case of symmetric rate limits, with $R^+_{max} = R^-_{max} = R_{max}$, the expression can be reduced to

$$\hat{P}_{sat} = P(|\dot{\beta}_1| > R_{max}) = 1 - \int_{-R_{max}}^{R_{max}} p_{\dot{\beta}_1}(\dot{\beta}_1, A, \sigma) d\dot{\beta}_1. \tag{34}$$

Therefore, similarly to the case of the ADC, once the pitch rate PDF has been reconstructed, the pitch rate saturation probability is obtained as the rate-limit exceedance likelihood for a given control configuration.

4 Validation

This section validates the presented methodology comparing its results with those given by aeroelastic simulations. The simulation setup is first described in Section 4.1. Then, Section 4.2 assesses the complete estimation of the pitch rate distribution by comparing the estimated SoR parameters with those from the turbulent simulations. Finally, in Section 4.3 the estimation of the actuatory duty cycle and rate saturation probability are assessed.

4.1 Simulation setup

The proposed methodology is validated using the IEA 15 MW Reference Wind Turbine in its offshore monopile configuration (Gaertner et al., 2020), whose main parameters are shown in Table 1. Aeroelastic simulations and model linearizations are performed with OpenFAST (Jonkman and Buhl, 2005). To capture the dominant aeroelastic couplings for simulation and control design, the model incorporates all the relevant degrees of freedom (DOFs). In this case, hydrodynamic effects are neglected by defining the sea state as still.

Table 1. Main parameters of the 15MW IEA reference wind turbine

Parameter	Units	Value
Rated Power	MW	15
Turbine Class	-	IEC 1B
Wind Speed Operation Range	m/s	3 – 25
Rated Wind Speed	m/s	10.59
Rotor Speed Range	rpm	5 – 7.56
Rotor Diameter	m	240
Pitch rate limit (R_{max})	deg/s	$\pm$ 2

The validation is carried out under turbulent inflow conditions generated with TurbSim (Jonkman, 2009) at an above-rated operating point corresponding to a mean wind speed of 19 m/s with a vertical shear exponent of 0.2. Ten independent seeds of IEC Class B normal turbulence (IEC Technical Committee, 2020) are simulated, each with a duration of 3600 seconds.

https://doi.org/10.5194/wes-2026-171
Preprint. Discussion started: 3 November 2026
© Author(s) 2026. CC BY 4.0 License.



eawe european academy of wind energy
Open Access WIND ENERGY SCIENCE DISCUSSIONS

The closed-loop architecture combines conventional collective pitch regulation with IPC. Rotor speed regulation is achieved through the collective controller

$$C_\Omega(s) = \frac{-0.0226(s+0.6341)}{s(s+2)}. \tag{35}$$

The IPC loop acts on the fixed-frame tilt and yaw load and employs identical controllers in the *dq* channels. To investigate the effect of different levels of asymmetric control activity on actuator utilization, two IPC tunings are considered,

$$C_{d_1}(s) = C_{q_1}(s) = \frac{-8.6\times10^{-6}}{s(s+12.57)}, \quad C_{d_2}(s) = C_{q_2}(s) = \frac{-8.6\times10^{-7}}{s(s+12.57)}, \tag{36}$$

hereafter referred to as IPC_1 and IPC_2, respectively. IPC_1 employs a controller gain on order of magnitude larger, resulting in a more aggressive asymmetric control action, greater load reduction capability and higher pitch activity. Conversely, IPC_2 provides a less aggressive action, with lower actuator demand but a more limited reduction of loads. The two configurations therefore provide representative cases with clearly differentiated levels of IPC activity for evaluating the proposed methodology.

4.2 pitch rate PDF estimation

This subsection validates the complete saturation probability estimation procedure by comparing its main steps with results obtained from turbulent aeroelastic simulations. The analysis first evaluates the estimation of the SoR distribution parameters A and σ. Finally, the resulting SoR-based saturation probabilities with those measured directly from the simulated pitch rate signals are compared.

The first step of the validation is focused on the deterministic SoR parameter A. Since the rotor speed is assumed to remain statistically close to its nominal value at the selected above-rated operating point, the validation focuses on the estimation of $\beta_{d,op}$ and $\beta_{q,op}$. These theoretical values, obtained from (21) and (22), respectively, are compared in Table 2 with the corresponding values from turbulent aeroelastic simulations. These values are computed by first obtaining the mean command for each turbulent realization and then averaging the results over all wind speeds.

Table 2. Comparison of the mean fixed-frame pitch commands and the deterministic SoR A parameter obtained from time-domain simulations (real) and predicted analytically (est.) for IPC_1 and IPC_2. The last two columns quantify the absolute and relative differences between the simulation based values obtained for both IPC configurations.

	IPC_1			IPC_2			Difference between IPC tunings	
Variable	**Real**	**Est.**	**|Rel.err.| (%)**	**Real**	**Est.**	**|Rel.err.| (%)**	$\lvert\Delta_{\text{IPC}}\rvert$	$\lvert\Delta_{\text{IPC,rel}}\rvert$ **(%)**
$\bar{\beta}_d$ (deg)	1.6758	1.6723	0.21	1.6701	1.6723	0.13	0.0057	0.34
$\bar{\beta}_q$ (deg)	−0.1916	−0.1895	1.10	−0.1871	−0.1895	1.29	0.0045	2.38
A (deg/s)	1.3354	1.3324	**0.23**	1.3305	1.3324	**0.14**	0.0049	0.37

Despite the difference in controller gains between the IPC_1 and IPC_2 configurations, the simulation based values of $\bar{\beta}_d$ and $\bar{\beta}_q$ remain similar. The relative difference $|\Delta_{\text{IPC,rel}}|$ is computed by normalizing their absolute difference by the average of

https://doi.org/10.5194/wes-2026-171
Preprint. Discussion started: 3 November 2026
© Author(s) 2026. CC BY 4.0 License.



eawe european academy of wind energy
Open Access WIND ENERGY SCIENCE DISCUSSIONS

their magnitudes. The resulting values are 0.34% and 2.38% for $\bar{\beta}_d$ and $\bar{\beta}_q$, respectively. The larger relative difference for $\bar{\beta}_q$ results partly from its comparatively small magnitude. Overall, these results support the assumption that the mean fixed frame pitch commands exhibit limited sensitivity to the IPC tuning.

The deterministic amplitude A also agrees closely with the analytical prediction. Relative estimation errors of 0.23% and 0.14% are obtained for IPC_1 and IPC_2, respectively, while the difference between both tunings is 0.37%. Therefore, the deterministic pitch rate contribution can be accurately characterized from the operating point quantities and the steady state gains of the linearized plant.

An important implication of this result is that the implementation of IPC inherently consumes part of the available actuator rate through the deterministic harmonic contribution. Since this contribution is periodic, the remaining rate margin available for turbulence-induced collective and IPC corrections is also time-varying. At the instants where the deterministic component reaches its maximum amplitude, the available margin is reduced from $R_{\max}$ to approximately $R_{\max} - A$.

Once the A parameter has been estimated, the next step concerns the estimation of the stochastic SoR parameter σ. As derived in Section 3.2.2, this parameter is obtained from the variance of the fluctuating blade pitch rate component, which depends on the variances and covariances of the fixed-frame pitch commands. Since these quantities can be computed from PSDs and CPSDs, the validation step consists of assessing the accuracy of the spectral estimation of the pitch comands in the *0dq* frame computed from the framework exposed in Section 2.2.

Figure 6 compares the PSDs of β_0, β_d and β_q obtained from turbulent aeroelastic simulations with those estimated using the equivalent-disturbance framework. The comparison is shown for both IPC configurations. By combining the equivalent disturbance PSDs with the closed-loop transfer functions of each controller, the proposed approach captures the different levels of pitch activity induced by the two IPC tunings. In particular, the larger spectral content observed in the *dq* axes for IPC_1 reflects the stronger asymmetric control action generated by this configuration, which is consistent with its higher controller gain.

The estimated PSDs are then used to compute the variance terms required in (26). Table 3 compares this quantities with the values obtained directly from the simulated time-domain signals. The results show that the proposed framework provides a consistent estimation of the individual variance contributions for both IPC configurations. Although some discrepancies appear in specific terms, the combined effect on the final stochastic parameter σ remains limited. The resulting absolute relative errors in this parameter are 4.44% for IPC_1 and 7.37% for IPC_2.

To further interpret the contribution of each term in (26), Figure 7 shows the relative weight of the different components involved in the computation of σ. For both IPC configurations, the dominant contribution is associated with the term related to the variance of β_d and β_q. This indicates that the variability of this commands, when projected into the rotating frame, is the main driver of the stochastic actuator-rate demand.

The relative contribution of each term depends on the level of IPC activity. For the less aggressive IPC_2 configuration, the collective pitch rate contribution represents almost the 20% of the total stochastic variance. In contrast, for the more aggresive IPC_1 configuration, this contribution decreases to around 5%, as the larger IPC gain shifts most of the variance towards the

https://doi.org/10.5194/wes-2026-171
Preprint. Discussion started: 3 November 2026
© Author(s) 2026. CC BY 4.0 License.

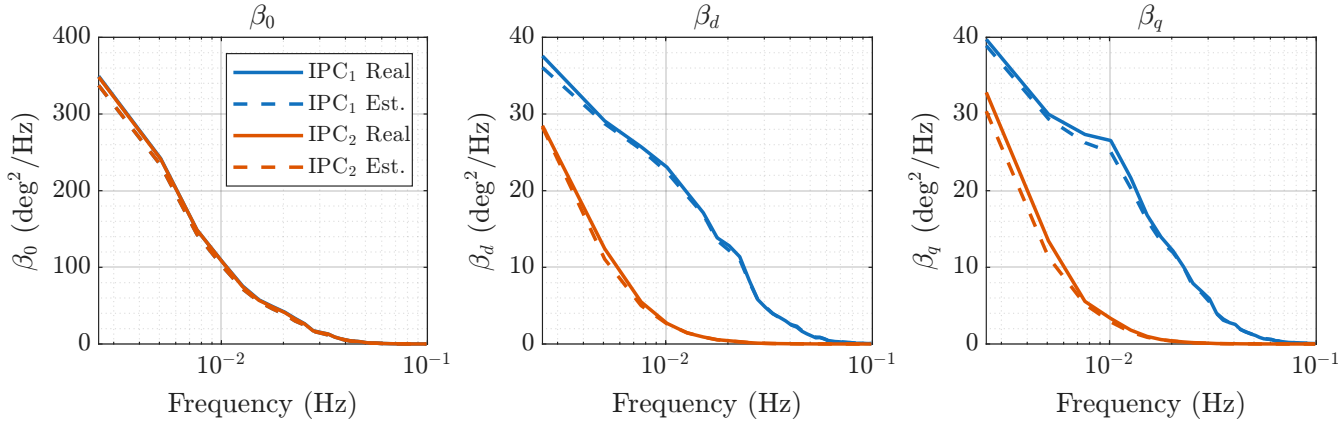


Figure 6. Comparison between simulated and estimated PSDs of the fixed-frame pitch commands β_0, β_d and β_q for IPC$_1$ and IPC$_2$. Solid lines correspond to turbulent aeroelastic simulations while dashed lines represent the estimated PSD using the equivalent-disturbance framework.

Table 3. Comparison between the separated and the total standard deviation obtained from time-domain simulations (real) and those estimated using the proposed framework (est.), under IPC$_1$ and IPC$_2$ control configurations.

	IPC$_1$			**IPC$_2$**		
Variable	**Real** (deg/s)	**Est.** (deg/s)	|**Rel. err.**| (%)	**Real** (deg/s)	**Est.** (deg/s)	|**Rel. err.**| (%)
σ_{β_d}	0.820	0.791	3.61	0.448	0.418	6.56
σ_{β_q}	0.833	0.788	5.47	0.462	0.422	8.79
$\sigma_{\dot{\beta}_0}$	0.163	0.153	6.17	0.162	0.152	5.95
$\sigma_{\dot{\beta}_d}$	0.166	0.151	9.07	0.021	0.020	5.44
$\sigma_{\dot{\beta}_q}$	0.159	0.145	8.71	0.021	0.020	6.81
σ	0.712	0.680	**4.44**	0.398	0.369	**7.37**

https://doi.org/10.5194/wes-2026-171
Preprint. Discussion started: 3 November 2026
© Author(s) 2026. CC BY 4.0 License.

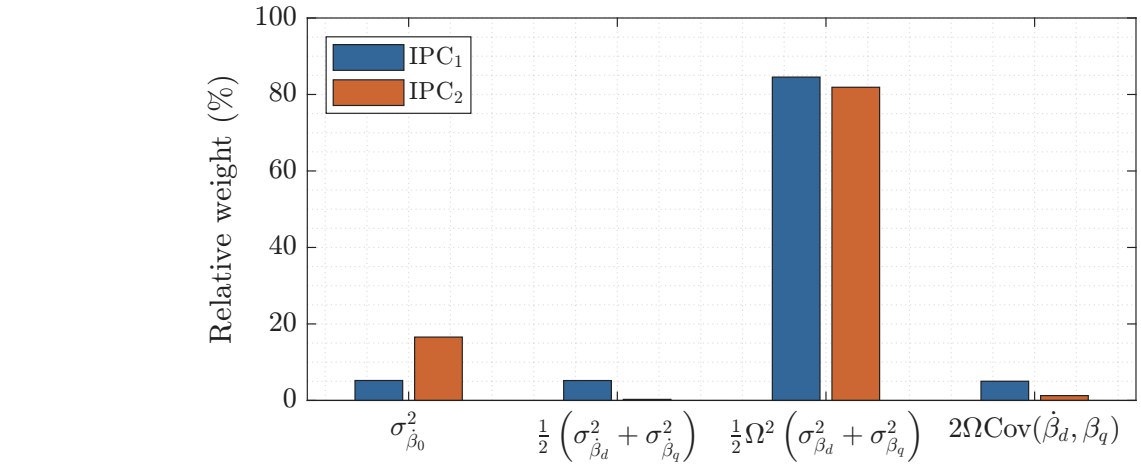
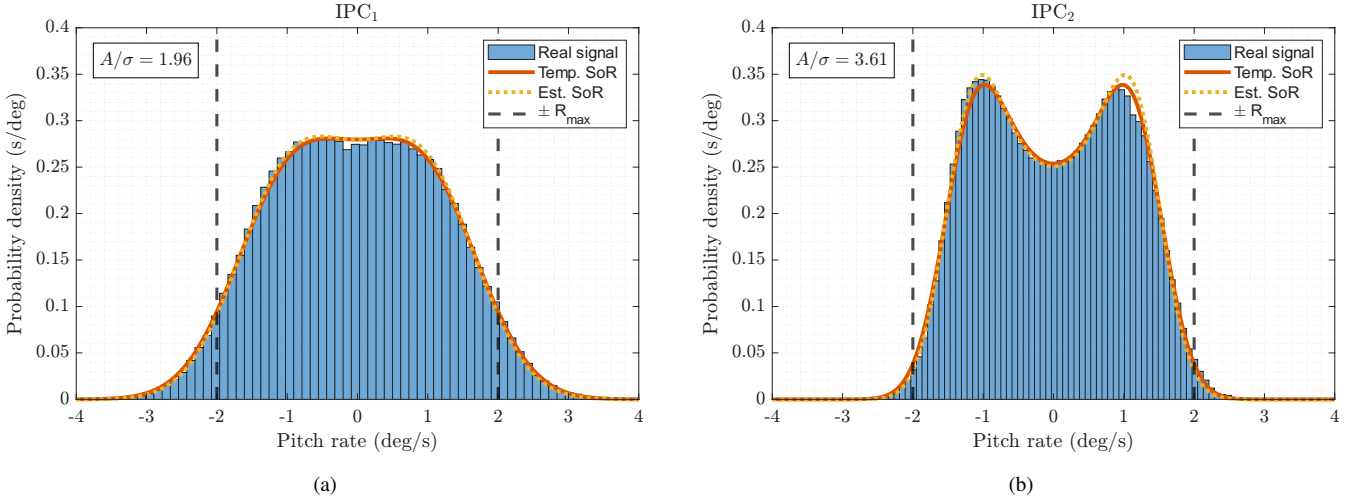


Figure 7. Relative contribution of each term in the analytical computation of the stochastic pitch rate variance σ for both IPC configurations.

asymmetric terms. All in all, these results emphasize that the accurate estimation fo the PSDs of β_d and β_q is essential for predicting the σ parameter.

Once A and σ parameters have been estimated, the pitch rate probability density function (PDF) can be built and compared with the distributions obtained from turbulent aeroelastic simulations. Figures 8a and 8b show the normalized histograms of the blade pitch rate signal for IPC_1 and IPC_2, respectively, together with two SoR reconstructions. The first one, denoted as temporal SoR, is obtained by computing the SoR parameters directly from the simulated time-domain signals. The second one, denoted as estimated SoR, is characterized using the parameters predicted by the proposed analytical and spectral framework.



(a) (b)

Figure 8. Normalized pitch rate histograms and SoR PDF reconstructions for IPC_1 (a) and IPC_2 (b), respectively. The temporal SoR is built from time-domain simulations signals, while the estimated SoR is characterized from the predicted parameters.

https://doi.org/10.5194/wes-2026-171
Preprint. Discussion started: 3 November 2026
© Author(s) 2026. CC BY 4.0 License.



eawe european academy of wind energy
Open Access WIND ENERGY SCIENCE DISCUSSIONS

The temporal SoR distributions reproduce the main shape of the simulated pitch rate histograms for both IPC configurations, supporting the suitability of the SoR model for representing pitch rate signals under IPC. The estimated SoR distributions also show good agreement with the simulated ones, indicating that the proposed estimation of A and σ provides a consistent reconstruction of the distribution of the signal.

The difference between the two IPC configurations is captured by the A/σ ratio. IPC_1 exhibits a more Gaussian-like distribution due to its larger relative contribution of the stochastic componente. In contrast, IPC_2 represents a distribution dominated by the deterministic component, indicating a stronger relative influence of the deterministic component. This behavior shows that, as the IPC action becomes more aggresive, the stochastic contribution of the turbulence to the pitch rate signal becomes dominant with respect to the deterministic component, converging in a more Gaussian-like distribution.

Although the graphical comparison provides a qualitative assessment of the distribution fit, a quantitative evaluation is presented in the following subsection. There, the actuator duty cycle and the rate saturation probability are computed from the reconstructed PDFs, where the resulting values are then compared with those obtained directly from time-domain turbulent simulations.

4.3 Actuator indicators estimation

Once the pitch rate PDF has been reconstructed, actuator related indicators can be computed directly from the distribution, as explained in Section 3.3. This subsection evaluates the prediction of actuator duty cycle and rate saturation probability by comparing the PDF-based estimates with the corresponding values obtained from turbulent aeroelastic simulations.

4.3.1 Actuatoy duty cycle

Following the procedure described in Section 3.3.1, ADC values are estimated for each control configuration. To provide a statistically consistent value representative of each control configuration, the reference ADC is computed as the average of the individual ADC values obtained from all turbulent simulations. Table 4 reports three values for each IPC configuration: the real ADC computed from the simulated pitch rate time signals, the ADC obtained from the SoR distribution parametrized with time-domain quantities and the ADC predicted using the estimated SoR parameters.

Table 4. Comparison of pitch actuator duty cycle from the aeroelastic simulations (**ADC Real**), the temporal SoR reconstruction (**ADC SoR**) and the estimated SoR reconstruction ($\widehat{\textbf{ADC}}$ **SoR**)

Control loop	**ADC Real** (%) (ref.)	**ADC SoR** (%)	$\lvert\textbf{Error}\rvert_{\textbf{Temp}}$ (%)	$\widehat{\textbf{ADC}}$ **SoR** (%)	$\lvert\textbf{Error}\rvert_{\textbf{Est}}$ (%)
$\textbf{IPC}_1$	49.24	49.15	**0.09**	48.45	**0.79**
$\textbf{IPC}_2$	44.35	44.30	**0.05**	44.07	**0.28**

The temporal SoR reconstruction shows excellent agreement with the simulation-based reference, with absolute errors of 0.09% for IPC_1 and 0.05% for IPC_2. This confirms that the SoR distribution provides an accurate representation of the temporal

https://doi.org/10.5194/wes-2026-171
Preprint. Discussion started: 3 November 2026
© Author(s) 2026. CC BY 4.0 License.



eawe european academy of wind energy
Open Access WIND ENERGY SCIENCE DISCUSSIONS

pitch rate signals. When the SoR parameters are estimated, the resulting ADC values remain close to their real value, with maximum absolute error below 0.8%.

These results demonstrate that the ADC can be predicted accurately from the characterized pitch rate PDF. Therefore, ADC can be evaluated during the linear control design stage without requering time-domain aeroelastic simulations for each IPC tuning.

4.3.2 Rate saturation probability

The final validation step evaluates the estimation of the pitch actuator rate saturation probability. For each simulation, this indicator is computed as the fraction of pitch rate values exceeding the positive or negative actuator rate limit. Like in the ADC case, to obtain a statistically consistent value representative of each control configuration, the resulting probabilities are averaged over all turbulent simulations. Table 5 compares the reference values obtained directly from the turbulent simulations with the temporal and estimated SoR distributions.

Table 5. Comparison of pitch saturation probability obtained from the aeroelastic simulations ($\mathbf{P_{sat}}$ **Real**), which serves as a reference, the temporal SoR reconstruction ($\mathbf{P_{sat}}$ **SoR**), and the estimated SoR reconstruction from the spectral framework ($\hat{\mathbf{P}}_{\mathbf{sat}}$ **SoR**), along with their relative errors respect to the reference for IPC_1 and IPC_2.

Control loop	$\mathbf{P_{sat}}$ **Real** (%) (ref.)	$\mathbf{P_{sat}}$ **SoR** (%)	$\lvert\mathbf{Error}\rvert_{\mathbf{Temp}}$ (%)	$\hat{\mathbf{P}}_{\mathbf{sat}}$ **SoR** (%)	$\lvert\mathbf{Error}\rvert_{\mathbf{Est}}$ (%)
$\mathbf{IPC_1}$	7.74	7.94	**0.20**	7.15	**0.59**
$\mathbf{IPC_2}$	1.39	1.32	**0.07**	0.95	**0.45**

The temporal SoR reconstruction provides saturation probabilities very close tho the simulation-based reference, with absolute errors of 0.2% for IPC_1 and 0.07% for IPC_2. This confirms that the SoR distribution accurately captures the probability density of the tails of the pitch rate distribution.

When the SoR parameters are estimated, the errors are 0.59% for IPC_1 and 0.45% for IPC_2, showing that the proposed method can estimate rate saturation probability with good accuracy using only operating point information, equivalent disturbance spectra and closed-loop transfer functions.

Overall, the validation of both ADC and P_{sat} confirms that the predicted pitch rate PDF provides a useful basis for evaluating actuator usage indicators during the linear control design stage, supporting decision-making during the loop-shaping, without requiring time-consuming, iterative aeroelastic simulations for each tuning.

5 Conclusions and Future Work

This work has presented a spectral methodology for predicting the probability density function of the pitch actuator rate under individual pitch control. The approach analytically decomposes the rotating frame pitch rate signal into a deterministic component and a stochastic contribution, allowing its statistical behaviour to be represented through a Sine-on-Random distribution.

https://doi.org/10.5194/wes-2026-171
Preprint. Discussion started: 3 November 2026
© Author(s) 2026. CC BY 4.0 License.



eawe european academy of wind energy
Open Access WIND ENERGY SCIENCE DISCUSSIONS

The parameters defining this distribution are estimated from operating point values, linear closed-loop transfer functions and the spectra of the equivalent wind disturbances. Once the pitch rate PDF is characterized, actuator indicators can be assessed during the linear control design stage. In this way, control design decisions can be made with reduced reliance on computationally expensive aeroelastic simulations.

The validation results support the representation of the pitch rate signal as a superposition of a deterministic and a Gaussian stochastic component. The resulting SoR PDF reproduce the pitch rate distribution obtained from turbulent aeroelastic simulations for both IPC configurations. In particular, the predicted PDFs capture the transition from a more aggressive controller with a Gaussian-like distribution to a milder control configuration in which the deterministic component become dominant. These results indicate that the estimated parameters A and σ adequately characterize the balance between deterministic component and corrective fluctuations.

The predicted pitch rate PDF enables the accurate estimation of actuator-related indicators. For the two IPC configurations, the actuator duty cycle is predicted with a maximum absolute error of 0.79%, while the maximum absolute error in the rate saturation probability is 0.59%. These results demonstrate that both actuator duty cycle and rate saturation probability can be assessed from the predicted PDF during the linear control desing stage.

The analytical decomposition also provides insight into the origin of the actuator rate demand under IPC. The mean dq pitch commands generate an inherent harmonic pitch rate component with amplitude A, which periodically occupies part of the available actuator rate capability regardless of the specific IPC tuning. The remaining rate margin is available for corrective collective and asymmetric actions. Moreover, the rotating frame projection of β_{dq} dominates the stochastic component, while the relative collective contribution depends on the aggressiveness of the IPC tuning making esential the accurate estimation of these fixed frame commands.

Future work will focus on incorporating the predicted actuator indicators into frequency-domain design specifications for methodologies such as Quantitative Feedback Theory (QFT) and H_∞, enabling controllers to be tuned towards prescribed ADC and P_{sat} targets. The proposed framework is also suitable for control co-design studies (Pao et al., 2024; Bayat et al., 2026), since the actuator rate capability R_{max} is explicitly included in the computation of both indicators, enabling controller parameters and actuator characteristics to be evaluated jointly, providing a basis for assessing trade-offs between control performance, actuator usage and actuator sizing. In addition, a quantitative relationship should be established between the predicted saturation probability and the resulting degradation of closed-loop performance indicators. Finally, future studies should assess how actuator saturation, once activated, modifies the closed-loop distribution and whether this feedback effect requires a corrected probabilistic model.

Code availability. The methods implemented in the code are described in detail in the paper to support transparency and reproducibility.

https://doi.org/10.5194/wes-2026-171
Preprint. Discussion started: 3 November 2026
© Author(s) 2026. CC BY 4.0 License.



eawe european academy of wind energy
Open Access WIND ENERGY SCIENCE DISCUSSIONS

Data availability. The data used in this study are simulated using open access tools. All models and procedures required to reproduce the data are described in the manuscript.

Author contributions. DLL: Conceptualization, formal analysis, methodology, validation, visualization, writing (original draft preparation). IMM: Conceptualization, writing (review and editing). JE: Conceptualization, writing (review and editing).

Competing interests. The authors declare that they have no conflict of interest.

Acknowledgements. The authors gratefully appreciate the support given by the Government of Navarre through the *Doctorados Industriales 2023* grant program number [0011-1408-2023-000013]. AI tools were used to improve the readability and linguistic quality of the manuscript. After using these tools, the authors reviewed and edited the content as needed and take full responsibility for the content of the published article.

https://doi.org/10.5194/wes-2026-171
Preprint. Discussion started: 3 November 2026
© Author(s) 2026. CC BY 4.0 License.



eawe european academy of wind energy
Open Access WIND ENERGY SCIENCE DISCUSSIONS

References

Aktan, H. D. and Bottasso, C. L.: Individual Pitch Control with a Reduced Actuator Duty Cycle*, in: 2023 IEEE Conference on Control Technology and Applications (CCTA), pp. 581–586, IEEE, Bridgetown, Barbados, ISBN 979-8-3503-3544-6, https://doi.org/10.1109/CCTA54093.2023.10252554, 2023.

Bayat, S., Peterson, C., Lee, Y. H., Iori, J., and Allison, J. T.: Advancing wind turbines through control co-design: An integrative review, Applied Energy, 416, 127 951, https://doi.org/10.1016/j.apenergy.2026.127951, 2026.

Bir, G.: Multi-Blade Coordinate Transformation and its Application to Wind Turbine Analysis, in: 46th AIAA Aerospace Sciences Meeting and Exhibit, American Institute of Aeronautics and Astronautics, Reno, Nevada, ISBN 978-1-62410-128-1, https://doi.org/10.2514/6.2008-1300, 2008.

Bossanyi, E. A.: Individual Blade Pitch Control for Load Reduction, Wind Energy, 6, 119–128, https://doi.org/10.1002/we.76, 2003.

Bossanyi, E. A.: Further load reductions with individual pitch control, Wind Energy, 8, 481–485, https://doi.org/10.1002/we.166, 2005.

Bottasso, C., Campagnolo, F., Croce, A., and Tibaldi, C.: Optimization-based study of bend–twist coupled rotor blades for passive and integrated passive/active load alleviation, Wind Energy, 16, 1149–1166, https://doi.org/10.1002/we.1543, 2013.

Bošnjaković, M., Katinić, M., Santa, R., and Marić, D.: Wind Turbine Technology Trends, Applied Sciences, 12, 8653, https://doi.org/10.3390/app12178653, 2022.

Canet, H., Bortolotti, P., and Bottasso, C. L.: On the scaling of wind turbine rotors, Wind Energy Science, 6, 601–626, https://doi.org/10.5194/wes-6-601-2021, 2021.

Feller, W.: An Introduction to Probability Theory and Its Applications, no. v. 1-2 in An Introduction to Probability Theory and Its Applications, Wiley, ISBN 978-0-471-25709-7, https://books.google.es/books?id=CDRMAAAAMAAJ, 1957.

Gaertner, E., Rinker, J., Sethuraman, L., Zahle, F., Anderson, B., Barter, G., Abbas, N., Meng, F., Bortolotti, P., Skrzypinski, W., Scott, G., Feil, R., Bredmose, H., Dykes, K., Shields, M., Allen, C., and Viselli, A.: Definition of the IEA 15-Megawatt Offshore Reference Wind Turbine, https://docs.nrel.gov/docs/fy20osti/75698.pdf, 2020.

Hammerum, K., Brath, P., and Poulsen, N. K.: A fatigue approach to wind turbine control, Journal of Physics: Conference Series, 75, 012 081, https://doi.org/10.1088/1742-6596/75/1/012081, 2007.

Henrique, A. I. D., Zhao, F., Backwell, B., Clarke, E., Ladwa, R., Jayasurya, F., Hutchinson, M., Williams, R., Han, W., Liang, W., Fang, E., Francisco, A. M., Shardul, M., Gitobu, J., Cheong, J., Muchiri, W., Fiestas, R., Rabie, H., Madan, K., Cargill, J., Lu, E., Sanchez, J. T., Melkonyan, N., Esteves, J., and Moreaux, B.: Global Wind Energy Council, Tech. rep., 2025.

Hovgaard, T. G., Caponetti, F., and Grunnet, J. D.: A Virtual Actuator for Advanced Individual Pitch Control (IPC), Journal of Physics: Conference Series, 2767, 032 009, https://doi.org/10.1088/1742-6596/2767/3/032009, 2024.

Hummel, J. I. S., Kober, J., and Mulders, S. P.: Output-constrained individual pitch control methods using the multiblade coordinate transformation: Trading off actuation effort and blade fatigue load reduction for wind turbines, https://doi.org/10.5194/wes-2024-153, 2025.

IEC Technical Committee: IEC 61400-1 Ed 3: Wind Turbines. Part 1, Design Requirements, 2020.

Jeong, M., Loth, E., Qin, C., Phadnis, M., Pusch, M., and Pao, L.: Operational Pitch Actuation Dynamics for Offshore Wind Turbines Ranging from 5 to 50 MW, Wind Energy, 28, e2975, https://doi.org/10.1002/we.2975, 2025.

Jonkman, B. J.: Turbsim User's Guide: Version 1.50, Tech. Rep. NREL/TP-500-46198, 965520, https://doi.org/10.2172/965520, 2009.

Jonkman, J. M. and Buhl, M. L. J.: FAST User's Guide - Updated August 2005, Tech. Rep. NREL/TP-500-38230, 15020796, https://doi.org/10.2172/15020796, 2005.

https://doi.org/10.5194/wes-2026-171
Preprint. Discussion started: 3 November 2026
© Author(s) 2026. CC BY 4.0 License.

Kanev, S.: Exploring the Limits in Individual Pitch Control, 2009.

Lacheta-Lecumberri, D., Miquelez-Madariaga, I., and Elso, J.: Fixed Frame Control-Oriented Modeling and Characterization of Asymmetric Wind Disturbances for Advanced Individual Pitch Control Design, https://doi.org/10.5194/wes-2026-134, 2026a.

Lacheta-Lecumberri, D., Miquelez-Madariaga, I., and Elso, J.: Spectral Methodology for Probabilistic Estimation of Pitch Actuator Rate Saturation in Wind Turbines, Journal of Physics: Conference Series, 3224, 052 007, https://doi.org/10.1088/1742-6596/3224/5/052007, 2026b.

Laks, J., Pao, L., Wright, A., Kelley, N., and Jonkman, B.: Blade Pitch Control with Preview Wind Measurements, in: 48th AIAA Aerospace Sciences Meeting Including the New Horizons Forum and Aerospace Exposition, American Institute of Aeronautics and Astronautics, Orlando, Florida, ISBN 978-1-60086-959-4, https://doi.org/10.2514/6.2010-251, 2010.

Liu, Y., Ferrari, R. M., and Van Wingerden, J.-W.: Periodic Load Rejection for Floating Offshore Wind Turbines via Constrained Subspace Predictive Repetitive Control, in: 2021 American Control Conference (ACC), pp. 539–544, IEEE, New Orleans, LA, USA, ISBN 978-1-6654-4197-1, https://doi.org/10.23919/ACC50511.2021.9483333, 2021.

Liu, Y., Ferrari, R., and Van Wingerden, J.-W.: Load reduction for wind turbines: an output-constrained, subspace predictive repetitive control approach, Wind Energy Science, 7, 523–537, https://doi.org/10.5194/wes-7-523-2022, 2022.

Ljung, L.: System Identification: Theory for the User, Prentice Hall PTR, 2nd edn., ISBN 0-13-656695-2, 1987.

Miquelez-Madariaga, I., Arellano, J., Lacheta-Lecumberri, D., and Elso, J.: Design of fatigue-based specifications for the design of controllers in wind turbines, Wind Energy Science, 11, 405–416, https://doi.org/10.5194/wes-11-405-2026, 2026.

Mulders, S. P., Pamososuryo, A. K., Disario, G. E., and Wingerden, J. V.: Analysis and optimal individual pitch control decoupling by inclusion of an azimuth offset in the multiblade coordinate transformation, Wind Energy, 22, 341–359, https://doi.org/10.1002/we.2289, 2019.

Pao, L. Y., Pusch, M., and Zalkind, D. S.: Control Co-Design of Wind Turbines, Annual Review of Control, Robotics, and Autonomous Systems, 7, 201–226, https://doi.org/10.1146/annurev-control-061423-101708, 2024.

Park, R. H.: Two-reaction theory of synchronous machines generalized method of analysis-part I, Transactions of the American Institute of Electrical Engineers, 48, 716–727, https://doi.org/10.1109/T-AIEE.1929.5055275, 1929.

Petrović, V., Jelavić, M., and Baotić, M.: MPC framework for constrained wind turbine individual pitch control, Wind Energy, 24, 54–68, https://doi.org/10.1002/we.2558, 2021.

Pusch, M., Phadnis, M., Jeong, M., Qin, C., Loth, E., and Pao, L.: Impact of Blade Pitch Actuation System on Wind Turbine Cost and Energy Production, Journal of Physics: Conference Series, 2767, 082 006, https://doi.org/10.1088/1742-6596/2767/8/082006, 2024.

Stephen O. Rice: Mathematical Analysis of Random Noise, 24, 46–156, https://doi.org/https://doi.org/10.1002/j.1538-7305.1945.tb00453.x, 1945.

Unguran, R., Petrovic, V., Pao, L. Y., and Kuhn, M.: Smart rotor control of wind turbines under actuator limitations, in: 2019 American Control Conference (ACC), pp. 3474–3481, IEEE, Philadelphia, PA, USA, ISBN 978-1-5386-7926-5, https://doi.org/10.23919/ACC.2019.8815001, 2019.

Vali, M., Van Wingerden, J.-W., and Kuhn, M.: Optimal multivariable individual pitch control for load reduction of large wind turbines, in: 2016 American Control Conference (ACC), pp. 3163–3169, IEEE, Boston, MA, USA, ISBN 978-1-4673-8682-1, https://doi.org/10.1109/ACC.2016.7525404, 2016.

https://doi.org/10.5194/wes-2026-171
Preprint. Discussion started: 3 November 2026
© Author(s) 2026. CC BY 4.0 License.



Wang, X. and Gambier, A.: Individual Pitch Control of a Large Wind Turbine Using a Fractional Order Nonlinear PI Approach with Anti-windup Strategy, in: 2021 IEEE Conference on Control Technology and Applications (CCTA), pp. 289–294, IEEE, San Diego, CA, USA, ISBN 978-1-6654-3643-4, https://doi.org/10.1109/CCTA48906.2021.9659118, 2021.

Zucca, G., Palmieri, M., and Cianetti, F.: On the statistical distribution of the maxima of sine on random process, Mechanical Systems and Signal Processing, 158, 107 726, https://doi.org/10.1016/j.ymssp.2021.107726, 2021.